ce/papers
The online collection for conference papers in civil engineering
Ernst & Sohn A Wiley Brand

ORIGINAL ARTICLE

SDSS 2022
The International Colloquium on Stability and Ductility of Steel Structures
14-16 September, University of Aveiro, Portugal
Ernst & Sohn A Wiley Brand

Numerical Investigation on the Thermal Behaviour of Steel-reinforced CFST Columns in Fire

David Medall[1], Ana Espinós[1], Vicente Albero[2], Carmen Ibáñez[1], Manuel L. Romero[1]

Correspondence

Dr Ana Espinós
Instituto de Ciencia y Tecnología del Hormigón (ICITECH)
Universitat Politècnica de València
Camino de Vera, s/n
46022 Valencia (Spain)
Email: aespinos@mes.upv.es

Abstract

In previous research, the authors highlighted the limited fire resistance of slender concrete-filled steel tubular (CFST) columns. A possible solution for enhancing the fire resistance of such columns consists of embedding an open steel profile within the concrete infill of the CFST section, generating the so-called steel-reinforced concrete-filled steel tubular (SR-CFST) section, where the inner steel profile results thermally protected by the surrounding concrete, thus delaying its degradation at elevated temperatures. This strategy may result beneficial in the fire situation as compared to other sectional configurations where the steel parts are directly exposed to the heat source.

In this paper, a two-dimensional finite element model will be developed for studying the thermal behaviour of SR-CFST columns and validated by comparing the temperature distribution results with experimental tests available in the literature. The numerical model will be subsequently used to carry out parametric studies, in order to analyse the influence of the different parameters, such as the cross-section shape, outer tube thickness or the inner steel profile sectional dimensions over the thermal response of these composite sections when subjected to fire.

Finally, a simplified temperature distribution proposal will be developed, which may help practitioners for a fast evaluation of the cross-sectional temperature field of SR-CFST columns at a given fire resistance period by assigning an equivalent temperature to each component of the composite section (hollow steel tube, concrete encasement and inner steel profile). This simplified temperature proposal may result helpful when evaluating the sectional capacity of SR-CFST columns in fire, by using a single strength and stiffness value for each component of the composite cross-section corresponding to its temperature.

Keywords

Steel-reinforced concrete-filled steel tubular columns, Fire resistance, Finite element model, Thermal analysis, Simplified temperature proposal.

1 Introduction

As discussed in previous investigations by the authors, concrete-filled steel tubular (CFST) columns have shown a premature failure when exposed to fire [1], which has led to the development of innovative solutions to improve the fire performance of these columns [2]. One of them consists of embedding a steel profile within the concrete of the CFST section, which results in the so-called steel-reinforced CFST section (SR-CFST). This configuration protects the inner profile thermally by the effect of the surrounding concrete, thus resulting in a lower thermal degradation and providing an enhanced mechanical capacity when exposed to fire.

A limited number of experimental investigations on the SR-CFST typology exposed to fire conditions can be found. Several research works were carried out by Chu et al. [3] and Zhu et al. [4]. Other experimental tests studied the residual capacity of SR-CFST columns after being exposed to elevated temperatures [5]. Additionally, Dotreppe et al. [6] carried out a series of experiments on unprotected columns and protected with intumescent paint.

Considering the experimental programs available in the literature, the amount of fire test results on SR-CFST columns is still limited. That is why numerous research groups have focused on studying their fire performance through numerical models, which were validated against the existing experiments in the literature [7-11]. Some of these analysis studied the influence of several parameters over the fire behaviour of SR-CFST columns, such as the outer tube material [9], the amount of steel placed inside the section [10] or the inner steel profile material [11].

1. Instituto de Ciencia y Tecnología del Hormigón (ICITECH), Universitat Politècnica de València, Valencia, Spain
2. Department of Mechanical Engineering and Construction, Universitat Jaume I, Castellón, Spain

https://doi.org/10.1002/cepa.1774

After a review of the literature, it has been found that there is no specific calculation method for these sections in the international design codes, therefore it is needed to find design equations that allow predicting the temperature distribution in SR-CFST sections. In this paper, a numerical model will be developed to derive design equations to allow practitioners easily predict the cross-sectional temperature distribution.

2 Development of the finite element model

A two-dimensional (2D) model was developed through the finite element analysis package ABAQUS [14]. As this research aims to study the thermal behaviour of SR-CFST columns uniformly exposed to fire, a 2D model is considered adequate.

2.1 Geometry and finite element mesh

The geometry of the section is constituted by three different assembled parts: the outer steel tube, the concrete infill, and the inner steel profile.

All of them are meshed using 3-node linear heat transfer triangles (DC2D3) with nodal temperature degree of freedom. A mesh sensitivity study was performed to obtain the optimal size of the finite elements. By simulating specimens 3A and 4A tested by Dotreppe et al. [6] with a FE of 5, 10 and 20 mm and comparing the precision of the numerically predicted temperatures, a 10 mm size was decided optimal in terms of accuracy and computational cost.

2.2 Boundary conditions at the exposed surface

In order to obtain the temperature field of the SR-CFST sections, a nonlinear heat transfer analysis was conducted in ABAQUS. When validating the model, the average temperature-time curve measured inside the furnace for each test was used, being this an important source of error in the validation process. In turn, the standard ISO-834 fire curve was applied to all the cases of the parametric studies.

The recommended values in EN 1991-1-2 [15] were adopted for the heat transfer parameters: a convective coefficient of α_c = 25 W/m^{2}K and an emissivity value ε = 0.7 were assumed at the exposed steel surface. Meanwhile, fire emissivity was set to ε = 1, and the Stephan-Boltzmann constant to σ = 5.67·10^{-8} W/m^{2}K^4.

2.3 Thermal contact at the steel concrete interface

When exposed to high temperatures, the outer steel tube separates transversely from the concrete infill due to the different thermal expansion of concrete and steel, which causes the appearance of physical space at the steel-concrete interface: an air gap.

The effect of this gap in the CFST section generates a thermal resistance and, therefore, a temperature difference between the outer steel tube and the concrete infill at the contacting surfaces, according to Ghojel [16]. Based on experimental data, Ghojel proposed an equation to estimate the thermal conductance of this gap in the case of circular and square CFST sections. More recently, Tao and Ghannam [17] proposed another expression that was dependent on the sectional dimensions of the column.

This thermal resistance was introduced in the numerical model via the "gap conductance" option in ABAQUS. A sensitivity study was performed, and based on its results, a constant gap conductance value of 200 W/m^{2}K was adopted, as used by the authors in previous investigations [18]. Fig. 1 shows the computed temperatures as compared to the experimental ones.

Even though the temperatures of the outer tube were similar under the three models, the monitored concrete-infill point was more precise assuming a constant gap conductance value and allowed a reduction in the computing demands of the model.

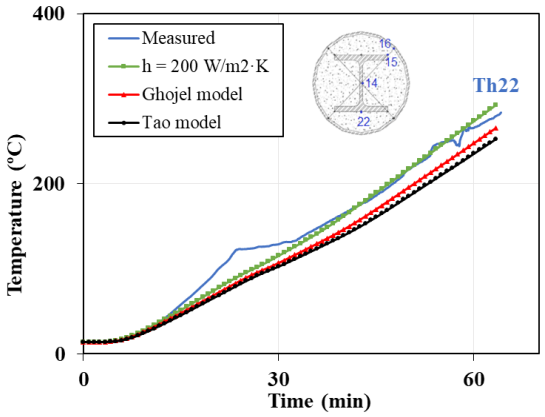

Figure 1 Sensitivity analysis on the "gap conductance" model. Comparison with case 3A tested by Chu et al. [3].

2.4 Material properties at high temperatures

Temperature dependant nonlinear material properties were used in the numerical model. For steel, the specific heat and thermal conductivity were modelled following the specifications given in EN 1993-1-2 [19].

The thermal properties for concrete at elevated temperatures were obtained from EN 1992-1-2 [20]. Nevertheless, the new expressions in the draft version of prEN 1992-1-2:2021-09 [21] were used to model the thermal conductivity of concrete, recommending a transition from the upper to the lower limit between 140 and 160 °C.

The latent heat of concrete water vaporisation was considered through a peak value in its specific heat formulation between 100 and 200 °C, as per Clause 3.3.2(8) in EN 1994-1-2 [13]. In those cases where no test data was provided, a moisture content value of 4% was assumed in the numerical model, as Clause 3.3.2(7) of EN 1994-1-2 [13] recommends.

3 Validation of the thermal model

Specimens 3A and 4A from the experimental results obtained by Chu at al. [3] were utilised to validate the numerical model. Moisture content was set to 6 %, as specified in Dotreppe et al. [6]. Additionally, tests 3B and 4B -protected with intumescent paint- were numerically simulated to extend the validation, even though fire-protected sections were not the aim of this research. Validation results of 3A and 4A specimens can be observed in Fig. 2.

Two circular (C2H and C4H) and four square (S1H, S2H, S3H, and S4) SR-CFST sections experimentally tested by Zhu et al. [4] were simulated with the numerical model. The embedded steel profile of all the sections has an HW 150 x 150 (150 mm × 150 mm × 7 mm × 10 mm) according to the Chinese standard GB706-2008.

For the non-uniformly exposed tests, a fiber blanket was introduced in the model with thermal conductivity of 0.1-0.2 W/m°C. The moisture content of 5% was used, according to Zhu et al. [4].

Table 1 summarises the main characteristics of the models used for the validation.

a)

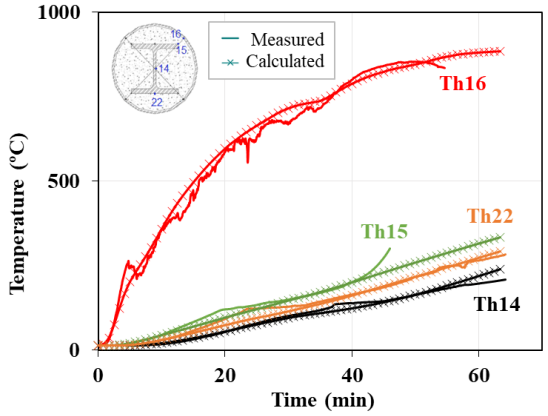

b)

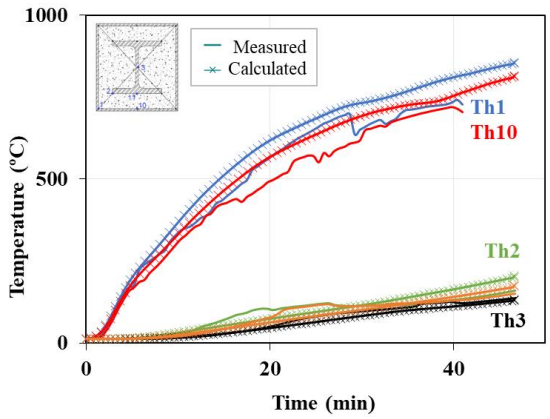

Figure 2 Comparison between measured and computed temperature-time curves for the case specimens tested by Chu et al. [3]: a) 3A, b) 4A.

3.1 Summary of the validation process

Fig. 3 summarises all the cases used for validation, where the predicted temperatures at the thermocouple locations are plotted at different standard fire times. The model is accurate enough, with most of its points laying within the ± 15% range, a mean value of 1.06 and a standard deviation of 25.78%. Prediction errors are calculated as T_{num}/T_{exp}.. It is also remarkable that, for temperatures above 300 °C, the model predictions are more precise obtaining a mean value of 1.04 and a standard deviation of 17.05%. This phenomenon may be explained by the evaporation of the concrete's moisture content, which occurs between 100-200 °C, causing a plateau in the temperature-time curves, a process difficult to replicate in the numerical model. Cases within the <300°C range have a mean value of 1.06 and a standard deviation of 29,60%. However, after this evaporation stage, the model shows excellent accuracy in predicting the temperature evolution.

Given the results obtained in the validation, the numerical model is deemed reliable for conducting parametric studies on SR-CFST-sections under high-temperature conditions, which will be discussed in the following section.

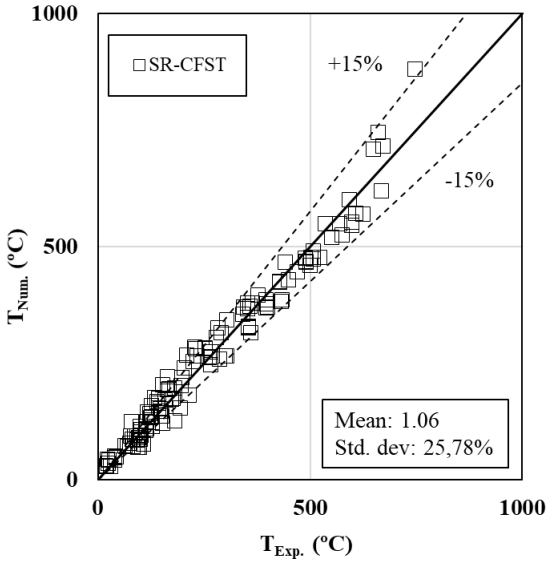

Figure 3 Numerically predicted temperatures versus experimental temperatures at the available thermocouple locations for the different cases used for validation.

Table 1 Geometrical and material characteristics of the SR-CFST column specimens used for validation.

	D x *t* *B* x *t* (mm)	$f_{y,tube}$ (MPa)	Internal profile	$f_{y,prof.}$ (MPa)	f_c (MPa)	Moisture
3A [3]	219.1x5	420	HEB120	375	35	6%
3B [3]	219.1x5	420	HEB120	375	35	6%
4A [3]	200x5	510	HEB120	375	35	6%
4B [3]	200x5	510	HEB120	375	35	6%
C4H [4]	300x8	360	HW150	345	55	5%
C2H [4]	300x8	360	HW150	345	55	5%
S4H [4]	300x6	360	HW150	345	55	5%
S3H [4]	300x6	360	HW150	345	55	5%
S2H [4]	300x6	360	HW150	345	55	5%
S1H [4]	300x6	360	HW150	345	55	5%

4 Parametric studies on the thermal response of SR-CFST columns

4.1 Selection of the composite sections for the parametric study

A parametric study was conducted to study the effects of several parameters on the cross-sectional capacity of SR-CFST columns under fire conditions.

The main parameters varied were the outer dimensions of the steel tube (*D* or *B* for circular and square, respectively), the steel tube thickness (*t*) and the inner steel profile dimensions.

Two groups of columns were analysed: eight sets of circular geometries and eight square-shaped sections. For comparison purposes, the outer tube dimensions were chosen to have the same amount of steel for all the circular-square counterparts with differences in steel area lower than 2%. For each hollow steel tubes two different wall thicknesses were studied: thin and thick. All the specimens were designed to meet the criteria of the non-slender sections (i.e. avoiding class 4), except for the CHS specimen with dimensions 500 mm x 8 mm. Two different inner steel profiles from the European wide flange beams catalog were considered for every steel tube: HEA and HEB. The dimensions of the inner steel profiles were progressively increased, so that for the wider tubes, two or three different inner profiles were studied.

In all, a total of 60 circular specimens and 60 square ones were simulated. Table 2 summarises all the columns included in the parametric study. The concrete moisture content was set to be 4% in all of the cases, as proposed in EN1994-1-2 [13]. The steel yield strength taken equal to 355 MPa, while the concrete compressive strength was assumed to be 30 MPa (calcareous aggregates considered).

4.2 Sectional integration

SR-CFST sections were discretised by employing a triangular mesh to conduct the thermal simulation in ABAQUS; thus, the temperature data was attained at every node of the FE mesh at evary time increment. These triangular elements can be characterised by their position (zi, yi), area (Ai), temperature (θ_i) - obtained by linear interpolation from its nodal temperatures- and the assigned material properties. Consequently, the cross-sectional plastic resistance and flexural stiffness at a specific fire exposure time can be obtained from the cell integration by using the following formula:

$$N_{fi,pl,Rd} = \sum_{i=1}^{n} A_{a,i} \cdot k_{y_a,\theta_i} \cdot f_{y_a} + \sum_{i=1}^{n} A_{c,i} \cdot k_{c,\theta_i} \cdot f_c + \sum_{i=1}^{n} A_{p,i} \cdot k_{y_p,\theta_i} \cdot f_{y_p} \quad (1)$$

$$EI_{z,fi} = \sum_{i=1}^{n} A_{a,i} \cdot y_i^2 \cdot k_{E_a,\theta_i} \cdot E_a + \sum_{i=1}^{n} A_{c,i} \cdot y_i^2 \cdot E_{c,sec,\theta_i} + \sum_{i=1}^{n} A_{p,i} \cdot y_i^2 \cdot k_{E_p,\theta_i} \cdot E_p \quad (2)$$

$$EI_{y,fi} = \sum_{i=1}^{n} A_{a,i} \cdot z_i^2 \cdot k_{E_a,\theta_i} \cdot E_a + \sum_{i=1}^{n} A_{c,i} \cdot z_i^2 \cdot E_{c,sec,\theta_i} + \sum_{i=1}^{n} A_{p,i} \cdot z_i^2 \cdot k_{E_p,\theta_i} \cdot E_p \quad (3)$$

where coefficients *a*, *c* and *p* correspond to the outer steel tube, concrete infill and inner steel profile, respectively.

$k_{y,\theta}$, $k_{c,\theta}$, $k_{E,\theta}$ are the temperature-dependent reduction factors that can be obtained from Table 3.2 and Table 3.3 in EN1994-1-2 [13] for steel and concrete. Additionally, the reduction factor for concrete elastic modulus (E_{c,sec,θ_i}) is not given in EN1994-1-2 [13]. However, it can be derived by using the following formula:

$$E_{c,sec,\theta_i} = \frac{f_{c,\theta_i}}{\varepsilon_{cu,\theta_i}} = \frac{k_{c,\theta_i}}{\varepsilon_{cu,\theta_i}} \cdot f_c \quad (4)$$

4.3 Analysis of the parametric study results

This section discusses the effect that the different parameters have over the fire performance of the columns. The following parameters will be analysed: the shape of the outer sections (circular and square), the outer tube thickness (cross-sectional slenderness), the section factor (A_m/V) and the inner steel profile dimensions (considered through the "Inner Steel Contribution Ratio" or A_p/A_c parameter).

4.3.1 Influence of the outer section shape

Fig. 4 compares the cross-sectional plastic resistance of the columns arranged by their total steel area (steel tube plus inner steel profile) for two standard fire exposure times: R30 and R120.

The trend is linearly positive, denoting an increase in the mechanical capacity of the column when the steel area is increased. Furthermore, the figure compares circular and square columns, showing that circular cross-sections perform slightly better when exposed to fire. This phenomenon is due to the smaller section factor of the circular sections, which implies a slower temperature rise. In addition, the lower concrete cover of the square sections results in the faster heating of the internal steel profile, reducing its mechanical properties. This effect is increased as fire exposure time rises, as can be observed in the difference between R30 and R120.

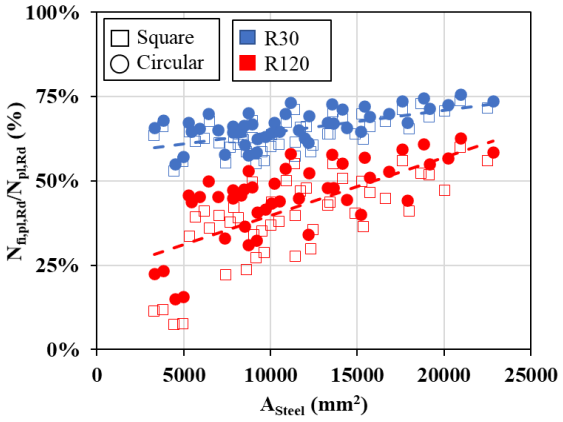

Figure 4 Influence of the total steel area over the cross-sectional plastic resistance of the columns for both circular and square sections.

4.3.2 Influence of the outer steel tube thickness

The correlation between the sectional plastic resistance of the column and the cross-section slenderness (*D/t*) is linearly positive, as is displayed in Fig. 5. As the *D/t* factor increases, the outer steel area diminishes, allowing for a higher concentration of concrete core and larger inner steel profile dimensions.

Because the outer tube is directly exposed to fire, it loses its load-bearing capacity rapidly but serves as a protection to inner parts of the column cross-section. Therefore, reducing the area of the outer steel tube and increasing the size of the thermally protected parts leads to an enhanced cross-sectional capacity.

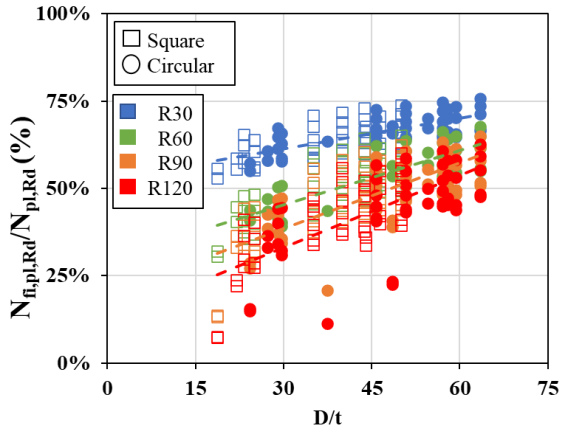

Figure 5 Influence of the cross-sectional slenderness (D/t) over the plastic resistance of the columns, for both circular and square sections.

4.3.3 *Influence of the section factor*

The section factor (A_m/V) was found to have a negative linear relation to the cross-sectional plastic resistance of the column, as displayed in Fig. 6. An increase of this parameter causes a higher exposed perimeter of the section, which leads to a faster heat-up of the column, consequently losing its mechanical properties as compared to less exposed columns. This effect is found to be amplified as the standard fire exposure time advances.

It is worth noting that, for the same steel usage, the section factor of the square columns is higher than that of their circular counterparts, which results in its faster temperature rise and mechanical deterioration.

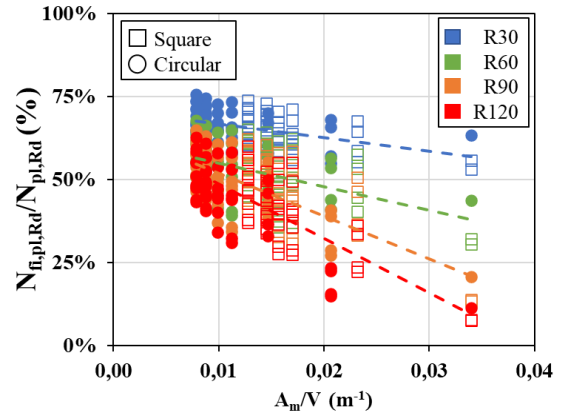

Figure 6 Influence of the section factor (A_m/V) over the cross-sectional plastic resistance of the columns for both circular and square sections.

4.3.4 *Influence of the inner steel profile dimensions*

The influence of the internal steel profile dimensions was analysed by selecting the most representative columns, simulated with a set of different embedded profiles. Fig. 7 compares the CHS 508 x 8 and the SHS 400 x 8 cases, with inner profiles HE100A, HE200A, HE300A, HE100B, HE200B, HE300B. All the cases were referred to the one with HE100A inner profile, to display the effect of an increased inner steel area. A new parameter was defined by the authors to compare the inner steel profile area to the concrete infill area, the so-called "Inner Steel Contribution Ratio" (ISCR): A_p/A_c.

The comparison shows that the cross-sectional capacity of the columns is enhanced when increasing the ISCR, for both circular and square sections at any given fire exposure time.

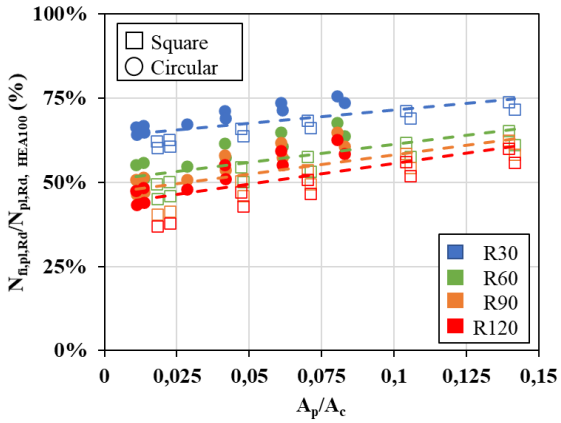

Figure 7 Influence of the Inner Steel Contribution Ratio (ISCR) over the cross-sectional plastic resistance of the columns for sections CHS 508 mm × 8 mm and SHS 400 mm × 8 mm.

Table 2 Summary of the analysis cases in the parametric studies

a) Circular sections		
D (mm)	**t (mm)**	**Inner profile**
193.7	4 8	HE100B
219.1	4 8	HE120B
273	5 10	HE140B
323.9	6 10	HE140B – HE180B
355.6	6 12.5	HE100B – HE200B
406.4	7 14.2	HE120B – HE220B
457	8 10	HE100 – HE180B – HE280B
508	8 10	HE100 – HE200B – HE300B

b) Square sections		
B (mm)	**t (mm)**	**Inner profile**
150	4 8	HE100B
175	4 8	HE120B
220	5 10	HE140B
260	6 10	HE140B – HE180B
300	6 12.5	HE100B – HE200B
325	7 14.2	HE120B – HE220B
350	8 10	HE100 – HE180B – HE280B
400	8 10	HE100 – HE200B – HE300B

5 Development of a simplified temperature distribution proposal for SR-CFST sections

When calculating the axial buckling load of steel-concrete composite columns, the design methods in EN 1994-1-2 [13] require obtaining previuosly the cross-sectional temperature distribution at a specific standard fire time. The desing code does not provide a simplified method to calculate the temperature field of the composite section in the case of SR-CFST columns. In the present section, a new proposal will be given to help designers in this task.

An equivalent temperature will be derived for each part of the composite cross-section: the outer steel tube ($\theta_{a,eq}$), the concrete infill ($\theta_{c,eq}$) and the web and flanges of the embed steel profile ($\theta_{w,eq}$ and $\theta_{f,eq}$). The authors successfully applied this same approach for obtaining the simplified temperature distribution in CFST columns in previous investigations [12].

5.1 Simplified cross-sectional temperature field

Using the numerical results of the previously conducted parametric studies, a multivariant nonlinerar regression analysis was conducted. The aim of this section is to provide a simplified method to obtain an equivalent temperature for each part of the composite cross-section of a SR-CFST column: the outer steel tube (θ_a), the concrete infill (θ_c) and the steel profile web (θ_w) and flanges (θ_f), see Fig. 8.

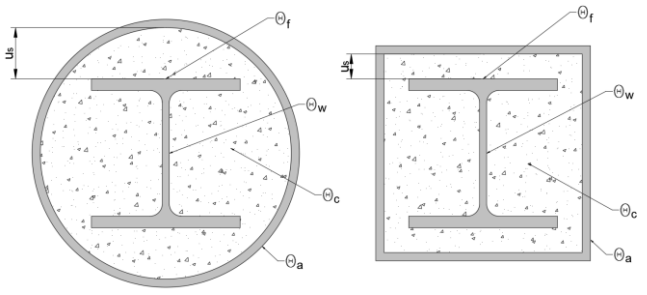

Figure 8 Equivalent temperatures of the different parts of the composite section and definition of the parameter u_s in circular and square SR-CFST sections.

5.1.1 *Calculation of the equivalent temperature for the outer steel tube*

The hollow steel tube temperature was obtained by the average of its inner and outer surface temperatures, which were directly obtained from the parametric study.

The previously proposed equivalent temperature of the outer tube for CFST columns given by the authors [12] was tested, obtaining an average error of 1.005 for the circular specimens and 1.021 for the square specimens with standard deviation values of 1.28% and 1.26%, respectively. The formula is given below:

$$\theta_{a,eq} = -824.667 - 5.579R + 0.007R^2 - 0.009R \cdot A_m/V + 645.076 \cdot R^{0.269} \cdot (A_m/V)^{0.017} \quad (5)$$

Fig. 8 shows a comparison between the numerically simulated and predicted temperatures for the outer tube, proving that the equation is well fitted for SR-CFST columns, showing a high correlation.

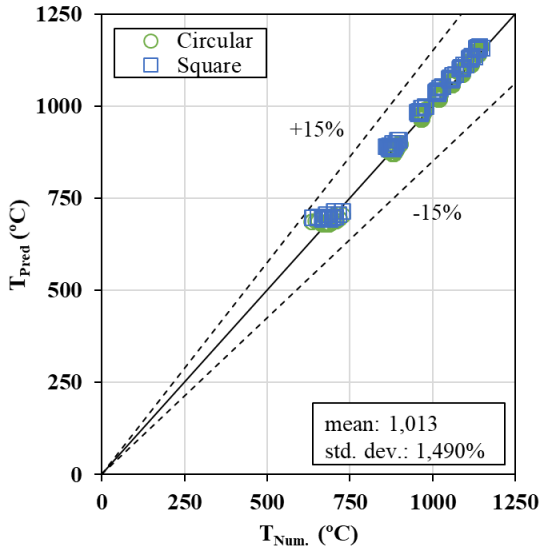

Figure 9 Comparison between predicted equivalent temperature and numerical temperature at the outer steel tube.

5.1.2 Calculation of the equivalent temperature for the concrete core

The equivalent temperature of the concrete core is obtained by two approaches: the plastic resistance or the flexural stiffness:

a) Plastic resistance approach

The plastic resistance of the concrete core at a specific temperature is

$$N_{fi,pl,Rd,c} = \sum_{i=1}^{n}(A_{c,i}\cdot f_{c,\theta_i}) = \sum_{i=1}^{n}(A_{c,i}\cdot k_{c,\theta_i}\cdot f_c) = f_c\cdot\sum_{i=1}^{n}(A_{c,i}\cdot k_{c,\theta_i}) \quad (6)$$

It is possible to isolate the reduction factor, which only depends on a single equivalent temperature of the concrete core:

$$N_{fi,pl,Rd,c} = f_c\cdot\sum_{i=1}^{n}(A_{c,i}\cdot k_{c,\theta_i}) = k_{c,\theta}(\theta_{c,eq1})\cdot f_c\cdot A_c \rightarrow k_{c,\theta}(\theta_{c,eq1}) = \frac{\sum_{i=1}^{n}(A_{c,i}\cdot k_{c,\theta_i})}{A_c} \quad (7)$$

Therefore, the equivalent temperature $\theta_{c,eq1}$ can be obtained by linearly interpolating in Table 3.3 in EN 1994-1-2 [20].

b) Flexural stiffness approach (major axis)

The flexural stiffness of the concrete core at elevated temperature can be calculated as:

$$EI_{z,fi,c} = \sum_{i=1}^{n}(I_{z,c,i}\cdot E_{c,sec,\theta_i}) = \sum_{i=1}^{n}(I_{z,c,i}\cdot\frac{f_{c,\theta,i}}{\varepsilon_{cu,\theta,i}}) = \frac{f_c}{\varepsilon_{cu}}\cdot\sum_{i=1}^{n}(I_{z,c,i}\cdot\frac{k_{c,\theta,i}}{\frac{\varepsilon_{cu,\theta,i}}{\varepsilon_{cu}}}) = E_{c,sec}\cdot\sum_{i=1}^{n}(I_{z,c,i}\cdot k_{Ec,\theta,i}) \quad (8)$$

with $k_{Ec,\theta,i} = k_{c,\theta,i}\cdot\varepsilon_{cu}/\varepsilon_{cu,\theta,i}$.

The equivalent temperature that produces the same reduction factor is then derived:

$$EI_{z,fi,c} = E_{c,sec}\cdot\sum_{i=1}^{n}(I_{z,c,i}\cdot k_{Ec,\theta,i}) = k_{Ec,\theta}(\theta_{c,eq2})\cdot E_{c,sec}\cdot I_{z,c} \rightarrow k_{Ec,\theta}(\theta_{c,eq2}) = \frac{\sum_{i=1}^{n}(I_{z,c,i}\cdot k_{Ec,\theta,i})}{I_{z,c}} \quad (9)$$

By applying this same procedure on the other axis, due to the column being not symmetrical, it is possible to obtain $\theta_{c,eq2}$ and $\theta_{c,eq3}$ from Table 3.3 in EN 1994-1-2 [20]. Through linear interpolation, considering $k_{Ec,\theta} = k_{c,\theta}\cdot\varepsilon_{cu}/\varepsilon_{cu,\theta}$.

Safely, the equivalent temperature of the concrete core will be considered as the higher of the three previously calculated ones:

$$\theta_{c,eq} = max\{\theta_{c,eq1},\theta_{c,eq2},\theta_{,eq3}\} \quad (10)$$

By using a multiple nonlinear regression, a single equation was developed for calculating the concrete core equivalent temperature:

$$\theta_{c,eq} = a_1 + b_1R + b_2R^2 + c_1(A_m/V) + c_2(A_m/V)^2 + d_1R(A_m/V) + e_1R^{f1}(A_m/V)^{f2} + g_1R(A_p/A_c) \leq 1200\ ºC \quad (11)$$

where the coefficients depend on the shape of the section and are included in Table 3. A comparison between the numerically calculated and predicted temperatures can be observed in Fig. 10.

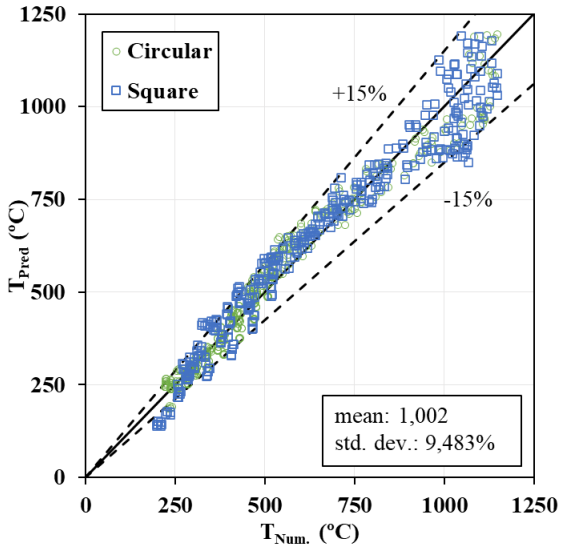

Figure 10 Comparison between predicted equivalent temperature and numerical temperature at the concrete core.

5.1.3 Calculation of the equivalent temperature of the inner steel profile

The temperatures of the inner steel profile differed significantly between the flanges and the web. Therefore, two different equivalent temperatures will be proposed, one for each part.

The process for obtaining the equivalent temperature of these parts was similar to that applied at the concrete core, including the plastic resistance and flexural stiffness approaches.

a) Plastic resistance approach

The axial compression plastic resistance of the different parts of the inner profile – web and flanges – under the effect of fire is:

$$N_{fi,pl,Rd,f} = \sum_{i=1}^{n}(A_{f,i}\cdot f_{s,\theta_i}) = \sum_{i=1}^{n}(A_{f,i}\cdot k_{s,\theta_i}\cdot f_s) = f_s\cdot\sum_{i=1}^{n}(A_{f,i}\cdot k_{s,\theta_i}) \quad (12)$$

$$N_{fi,pl,Rd,w} = \sum_{i=1}^{n}(A_{w,i}\cdot f_{s,\theta_i}) = \sum_{i=1}^{n}(A_{w,i}\cdot k_{s,\theta_i}\cdot f_s) = f_s\cdot\sum_{i=1}^{n}(A_{w,i}\cdot k_{s,\theta_i}) \quad (13)$$

The reduction factor id subsequently derived:

$$N_{fi,pl,Rd,f} = f_s \cdot \sum_{i=1}^{n}(A_{f,i} \cdot k_{s,\theta_i}) = k_{s,\theta}(\theta_{f,eq1}) \cdot f_s \cdot A_f \rightarrow k_{s,\theta}(\theta_{f,eq1}) = \frac{\sum_{i=1}^{n}(A_{f,i} \cdot k_{s,\theta_i})}{A_f} \quad (14)$$

$$N_{fi,pl,Rd,w} = f_s \cdot \sum_{i=1}^{n}(A_{w,i} \cdot k_{s,\theta_i}) = k_{s,\theta}(\theta_{w,eq1}) \cdot f_s \cdot A_w \rightarrow k_{s,\theta}(\theta_{w,eq1}) = \frac{\sum_{i=1}^{n}(A_{w,i} \cdot k_{s,\theta_i})}{A_w} \quad (15)$$

By linear interpolation in Table 3.2 in EN 1994-1-2 [13], the equivalent temperatures $\theta_{f,eq1}$ and $\theta_{w,eq1}$ can be then obtained.

b) Flexural stiffness approach (major axis)

The flexural stiffness of both flanges and web at a given temperature for major axis bending can be obtained by the following formula:

$$EI_{z,fi,f} = \sum_{i=1}^{n}(I_{z,f,i} \cdot E_{a,\theta}) = \sum_{i=1}^{n}(I_{z,f,i} \cdot k_{E,\theta}(\theta_{f,eq2}) \cdot E_a) = E_a \cdot \sum_{i=1}^{n}(I_{z,f,i} \cdot k_{E,\theta}(\theta_{f,eq2})) \quad (16)$$

$$EI_{z,fi,w} = \sum_{i=1}^{n}(I_{z,w,i} \cdot E_{a,\theta}) = \sum_{i=1}^{n}(I_{z,w,i} \cdot k_{E,\theta}(\theta_{w,eq2}) \cdot E_a) = E_a \cdot \sum_{i=1}^{n}(I_{z,w,i} \cdot k_{E,\theta}(\theta_{w,eq2})) \quad (17)$$

After that, it is possible to obtain the reduction coefficient:

$$EI_{z,fi,f} = E_a \cdot \sum_{i=1}^{n}(I_{z,f,i} \cdot k_{E,\theta}(\theta_{f,eq2})) = k_{E,\theta}(\theta_{f,eq2}) \cdot E_a \cdot I_{z,f} \rightarrow k_{E,\theta}(\theta_{f,eq2}) = \frac{\sum_{i=1}^{n}(I_{z,f,i} \cdot k_{E,\theta,i})}{I_{z,f}} \quad (18)$$

$$EI_{z,fi,w} = E_a \cdot \sum_{i=1}^{n}(I_{z,w,i} \cdot k_{E,\theta}(\theta_{w,eq2})) = k_{E,\theta}(\theta_{w,eq2}) \cdot E_a \cdot I_{z,w} \rightarrow k_{E,\theta}(\theta_{w,eq2}) = \frac{\sum_{i=1}^{n}(I_{z,w,i} \cdot k_{E,\theta,i})}{I_{z,w}} \quad (19)$$

The same process is applied to the minor bending axis. Equivalent temperatures $\theta_{f,eq2}$, $\theta_{w,eq2}$, $\theta_{f,eq2}$ and $\theta_{w,eq3}$ are obtained from Table 3.2 in EN 1994-1-2 [13] by linear interpolation.

Conservatively, the equivalent temperatures for each part of the inner steel profile are:

$$\theta_{f,eq} = max\{\theta_{f,eq1,}\ \theta_{f,eq2}, \theta_{f,eq3}\} \quad (20)$$

$$\theta_{w,eq} = max\{\theta_{w,eq1,}\ \theta_{w,eq2}, \theta_{w,eq3}\} \quad (21)$$

Equivalent temperature for the flanges of the inner steel profile

To calculate the equivalent temperature oft he inner profile flanges, a parameter was defined to represent the concrete cover around the flange. Parameter u_s measures the distance between the flanges of the embedded steel profile and the inner surface of the hollow steel tube, as shown in Fig. 8.

Thus, a multiple nonlinear regression analysis was performed, obtaining the following equation for the equivalent temperature of the inner steel profile flanges:

$$\theta_{f,eq} = a_1 + b_1 R + b_2 R^2 + c_1(A_m/V) + c_2(A_m/V)^2 + d_1 R(A_m/V) + e_1 R^{f1}(A_m/V)^{f2} + g_1 u_s \quad (22)$$

where the coefficients depend on the shape of the column; see Table 3. Fig 11 compares the calculated versus the predicted temperatures at the inner steel profile flanges.

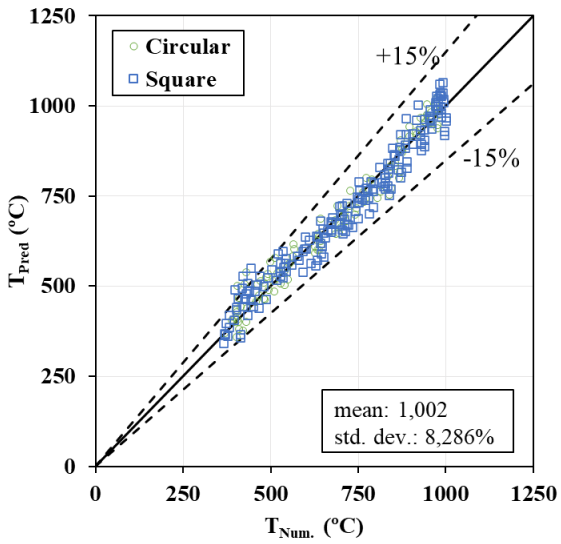

Figure 11 Comparison between predicted equivalent temperature and numerical temperature at the inner steel profile flanges.

Equivalent temperature for the web of the inner steel profile

When characterising the web temperature of the inner steel profile, the ISCR was shown to be relevant in the regression analysis. Therefore, a formula is obtained including this parameter:

$$\theta_{w,eq} = a_1 + b_1 R + b_2 R^2 + c_1(A_m/V) + c_2(A_m/V)^2 + d_1 R(A_m/V) + e_1 R^{f1}(A_m/V)^{f2} + g_1(A_p/A_c) + g_2(A_p/A_c)^2 \quad (23)$$

where coefficients depend on the cross-section shape, see Table 3. A comparison is performed between the numerically calculated and predicted temperatures of the web and is included in Figure 12.

Table 3 Coefficients for the equivalent temperature equations of the concrete core $\theta_{c,eq}$ (°C), inner steel profile flanges $\theta_{f,eq}$ (°C) and web $\theta_{w,eq}$ (°C)

		a_1	b_1	b_2	c_1	c_2	d_1	e_1	f_1	f_2	g_1	g_2
$\theta_{c,eq}$	CIRC	1120,110	-10,143	7,804E-03	-145,937	4,049	1,299	-1,832E-05	1,905	2,842	5,170	-
	SQUA	865,598	-23,880	2,910E-02	-93,380	1,549	5,884	-1,541	1,093	1,202	4,704	-
$\theta_{f,eq}$	CIRC	-1174,15	14,079	-2,025E-02	59,591	2,120E-02	-5,835E-02	9,529E-05	1,827	1,862	9,269	-
	SQUA	794,251	-7,188	9,833E-03	-81,303	1,258	7,589	-4,506	1,047	1,061	-9,638	-
$\theta_{w,eq}$	CIRC	3267,34	3,242	0,0125	184,789	-5,301	3,594	-1,286	1,175	1,010	10891,6	-55465,4
	SQUA	-941,091	-5,318	6,62E-03	-22,252	0,358	3,411	-1,173	1,098	1,124	6939,91	-19679,4

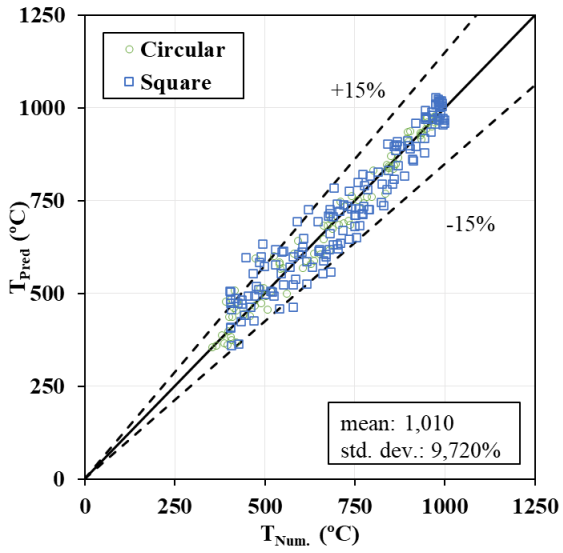

Figure 12 Comparison between predicted equivalent temperature and numerical temperature at the inner steel profile web.

5.2 Applicability limits of the proposed method

The presented method should only be used for SR-CFST columns that meet the following criteria:

- For circular SR-CFST columns:

$$8\ m^{-1} \leq A_m/V \leq 20\ m^{-1}$$

$$24 \leq D/t \leq 64$$

$$0{,}011 \leq A_p/A_c \leq 0{,}108$$

- For square SR-CFST columns:

$$13\ m^{-1} \leq A_m/V \leq 34\ m^{-1}$$

$$19 \leq B/t \leq 50$$

$$0{,}018 \leq A_p/A_c \leq 0{,}204$$

- Standard fire exposure times between 30 and 240 minutes.

6 Summary and conclusions

In this paper, a two-dimensional finite element model was developed and validated against the experimental cases available in the literature by using the nonlinear analysis software package ABAQUS.

The model was used to perform a parametric study comprising 120 case specimens, which were subjected to a heat transfer analysis through the developed numerical model. Once the thermal analysis of all the sections had been conducted, an automatized numerical integration procedure was conducted by the authors to obtain the plastic resistance and flexural stiffness of the different parts of the columns at a specific fire exposure time. The influence of multiple parameters over the plastic resistance of the cross-section was studied, being these parameters the section shape (circular or square), the outer steel tube thickness, the section factor (A_m/V) and the Inner Steel Contribution Ratio (ISCR).

It was found that, for the same steel usage, the circular columns performed better under fire conditions due to the higher section factors of the square columns, thus explaining their faster mechanical degradation. Both the reduction of the outer steel tube thickness and the increase of the inner steel profile dimensions enhanced the mechanical capacity of the columns at high temperatures. The increment in the ISCR ratio was also found to improve the fire performance of the columns.

With the help of a statistical processing of the data from the parametric studies, an innovative method for calculating the simplified temperature field of SR-CFST columns under ISO-834 standard fire conditions was developed. This proposal provides practitioners with a user-friendly tool to easily obtain the equivalent temperatures at each part of the composite cross-section. Equations are provided for this means.

The method presented in this paper covers an existing limitation in EN 1994-1-2 for the fire design of certain types of steel-concrete composite sections, such as SR-CFST columns.

Acknowledgements

The authors would like to express their sincere gratitude for the help provided through the Grant PID2019-105908RB-I00 and for the first author's pre-doctoral contract through the Grant PRE2020-093106 funded by MCIN/AEI/ 10.13039/501100011033 and by "ESF Investing in your future".

References

[1] Espinos A, Romero ML, Serra E, Hospitaler A. Circular and square slender concrete-filled tubular columns under large eccentricities and fire. Journal of Constructional Steel Research 2015. https://doi.org/10.1016/j.jcsr.2015.03.011.

[2] Romero ML, Espinós A, Lapuebla-Ferri A, Albero V, Hospitaler A. Recent developments and fire design provisions for CFST columns and slim-floor beams. Journal of Constructional Steel Research 2020;172:106159. https://doi.org/10.1016/j.jcsr.2020.106159.

[3] Chu TB, Gernay T, Dotreppe J-C, Franssen J. Steel hollow columns with an internal profile filled with self-compacting concrete under fire conditions. 2016.

[4] Zhu Meichun, Meng Fanqin, He Baojie. Experimental research on fire resistance of steel tubular columns filled with steel reinforced concrete. Journal of Building Structures 2016;37:36–43.

[5] Meng F, Zhu M-C, Mou B, He B. Residual Strength of Steel-Reinforced Concrete-Filled Square Steel Tubular (SRCFST) Stub Columns After Exposure to ISO-834 Standard Fire. International Journal of Steel Structures 2019;19:850–66. https://doi.org/10.1007/s13296-018-0174-z.

[6] Claude Dotreppe J, Binh Chu T, Eng R, Marc Franssen J. Steel hollow columns filled with self-compacting concrete under fire conditions. 2010.

[7] Meng F-Q, Zhu M-C, Clifton GC, Ukanwa KU, Lim JBP. Performance of square steel-reinforced concrete-filled steel tubular columns subject to non-uniform fire. Journal of Constructional Steel Research 2020;166. https://doi.org/10.1016/j.jcsr.2019.105909.

[8] Fan-Qin Meng, Mei-Chun Zhu, G. Charles Clifton, Kingsley U. Ukanwa, James B.P. Lim. Fire performance of edge and interior circular steel-reinforced concrete-filled steel tubular stub columns. Steel and Composite Structures 2021;41:115–22.

[9] Tan Q-H, Gardner L, Han L-H, Song T-Y. Fire performance of steel reinforced concrete-filled stainless steel tubular (CFSST) columns with square cross-sections. Thin-Walled Structures 2019;143. https://doi.org/10.1016/j.tws.2019.106197.

[10] Espinos A, Romero ML, Lam D. Fire performance of innovative steel-concrete composite columns using high strength steels. Thin-Walled Structures 2016;106:113–28. https://doi.org/10.1016/j.tws.2016.04.014.

[11] Mao W-J, Wang W-D, Xian W. Numerical analysis on fire performance of steel-reinforced concrete-filled steel tubular columns with square cross-section. Structures 2020;28:1–16. https://doi.org/10.1016/j.istruc.2020.08.043.

[12] Albero V, Espinos A, Romero ML, Hospitaler A, Bihina G, Renaud C. Proposal of a new method in EN1994-1-2 for the fire design of concrete-filled steel tubular columns. Engineering Structures 2016;128:237–55. https://doi.org/10.1016/j.engstruct.2016.09.037.

[13] CEN. EN 1994-1-2, Eurocode 4: Design of composite steel and concrete structures. Part 1.2: General rules - Structural fire design. 2005.

[14] Abaqus/CAE User's Guide. Version 2019. 2019.

[15] CEN. EN 1991-1-2, Eurocode 1: Actions on structures - Part 1-2: General actions - Actions on structures exposed to fire. 2002.

[16] Ghojel J. Experimental and analytical technique for estimating interface thermal conductance in composite structural elements under simulated fire conditions. Experimental Thermal and Fluid Science 2004;28:347–54.

[17] Tao Z, Ghannam M. Heat transfer in concrete-filled carbon and stainless steel tubes exposed to fire. Fire Safety Journal 2013;61:1–11. https://doi.org/10.1016/J.FIRESAF.2013.07.004

[18] Espinos A, Romero ML, Hospitaler A. Advanced model for predicting the fire response of concrete filled tubular columns. Journal of Constructional Steel Research 2010. https://doi.org/10.1016/j.jcsr.2010.03.002.

[19] CEN. EN 1993-1-2, Eurocode 3: Design of steel structures, Part 1.2: General rules – Structural fire design. 2005.

[20] CEN. EN 1992-1-2, Eurocode 2: Design of concrete structures, Part 1.2: General rules – Structural fire design. 2004.

[21] CEN/TC250/SC2 N1897 - Stable version prEN 1992-1-2:2021-09. Eurocode 2: Design of concrete structures - Part 1-2: General rules - Structural fire design. 2021.